Evidence for thermal boundary resistance effects on superconducting radiofrequency cavity performances

2014 Supercond. Sci. Technol. 27 085004

(http://iopscience.iop.org/0953-2048/27/8/085004)

OPEN ACCESS
IOP Publishing
Superconductor Science and Technology
Supercond. Sci. Technol. **27** (2014) 085004 (11pp)
doi:10.1088/0953-2048/27/8/085004

Evidence for thermal boundary resistance effects on superconducting radiofrequency cavity performances

Vincenzo Palmieri[1], **Antonio Alessandro Rossi**[1], **Sergey Yu Stark**[1] and **Ruggero Vaglio**[2]

[1] Laboratori Nazionali di Legnaro, Istituto Nazionale di Fisica Nucleare, Legnaro, Italy
[2] CNR-SPIN and University of Napoli Federico II, Italy

E-mail: palmieri@lnl.infn.it

Received 13 February 2014, revised 12 April 2014
Accepted for publication 13 May 2014
Published 25 June 2014

Abstract

The majority of the literature on superconducting cavities for particle accelerators concentrates on the interaction of a radiofrequency (RF) electromagnetic field with a superconductor cooled in liquid helium, generally either at a fixed temperature of 4.2 K or 1.8 K, basing the analysis of experimental results on the assumption that the superconductor is at the same temperature as the infinite reservoir of liquid helium. Only a limited number of papers have extended their analysis to the more complex overall system composed of an RF field, a superconductor and liquid helium. Only a few papers have analyzed, for example, the problem of the Kapitza resistance, i.e. the thermal boundary resistance between the superconductor and the superfluid helium. Among them, the general conclusion is that the Kapitza resistance, one of the most controversial and less understood topics in physics, is generally negligible, or not relevant for the performance enhancement of cavities. In our work presented here, studying the performance of 6 GHz niobium (Nb) test cavities, we have discovered and studied a new effect consisting of an abrupt change in the surface resistance versus temperature at the superfluid helium lambda transition T_λ. This abrupt change (or 'jump') clearly appears when the RF measurement of a cavity is performed at constant power rather than at a constant field. We have correlated this jump to a change in the thermal exchange regime across the lambda transition, and, through a simple thermal model and further reasonable assumptions, we have calculated the thermal boundary resistance between niobium and liquid helium in the temperature range between 4.2 K and 1.8 K. We find that the absolute values of the thermal resistance both above and below the lambda point are fully compatible with the data reported in the literature for heat transfer to pool boiling helium I (He_I) above T_λ and for the Kapitza interface resistance (below T_λ) between a polished metal surface and superfluid He_{II}. Finally, based on the well-documented evidence that the surface status of metal to liquid helium influences the heat exchange towards the fluid, and specifically the Kapitza resistance below T_λ, we have tested an anodization process external to the cavity, comparing the performances of the cavity before and after external anodization. The tests were done without breaking the vacuum inside the cavity or modifying the inner superconducting layer in any way, and were repeated on different samples. The results show that when the cavity is externally anodized, both the Q-factor and the maximum accelerating field increase. Again, when the oxide layer is removed, the Q-factor shifts towards a lower level and the maximum accelerating field is also reduced.

Keywords: Kapitza resistance, thermal boundary resistance, superconducting cavities, niobium, liquid helium, lambda transition of superfluid helium

(Some figures may appear in colour only in the online journal)

1. Introduction

The optimization of superconducting radiofrequency (RF) cavity performance is still a relevant issue for future particle accelerator development. The main parameters are the absolute value of the cavity quality factor Q, the maximum value of the accelerating electric field (breakdown field) and the 'Q-slope', i.e. the level of degradation of Q for increasing values of the accelerating field.

If the applied RF field can be considered homogeneous over the cavity surface, the quality factor Q is directly related to the superconductor surface resistance R_s by the relation $Q = \Gamma/R_s$, where Γ is a constant related to the cavity geometry (temperature- and field-independent).

The surface resistance at zero field is usually written as the sum of two terms:

$$R_s(T) = R_{BCS}(T) + R_0. \tag{1}$$

R_{BCS} (T) is the 'ideal' theoretical, strongly temperature-dependent, surface resistance as given by the BCS theory and R_0 is a temperature-independent residual term that accounts for a large set of possible 'spurious' effects [1]. Since the BCS term goes to zero at low temperatures, this last term generally dominates at very low temperatures and at low frequency.

The BCS term has a fairly complex expression that needs to be computed numerically [2]. In specific conditions (low frequency in respect to the gap frequency, dirty and local limits, temperature $T \ll T_c$) some approximations can be made, leading to the simplified expression:

$$R_{BCS}(T) = \frac{A\omega^2}{T} \exp\left(-\frac{\Delta_0}{K_B T}\right) \tag{2}$$

(where Δ_0 is the low temperature value of the energy gap, K_B is the Boltzmann constant and A is a weak frequency-dependent constant, whose value is determined by the material parameters [3, 4].

Equation (2) is generally assumed to be valid for standard accelerating cavities and essentially almost all papers in the field use this expression for the BCS term to fit the data.

The power dissipated by the RF field per unit area over a depth λ from the cavity inner surface (λ is the magnetic field penetration depth, generally less than 100 nm) can be written as:

$$P_d = \frac{1}{2} R_s(T) H_{RF}^2 \tag{3}$$

where H_{RF} is the amplitude of the RF magnetic field. The corresponding magnetic induction $\mu_0 H_{RF}$ is directly proportional to the accelerating field E_{acc}, through a constant that is equal to 4.5 mT/(MV/m) for the elliptical cavities of the TESLA design [1] accelerating relativistic electrons (v/c = 1).

If surface resistance were independent of field level, a cavity characterization measurement would reveal a flat response of Q versus E_{acc} up to a certain critical field. In practice the Q-factor versus field tends to decay with a severe or less severe slope, depending on the case, implying a field-dependent surface resistance (increasing with the field amplitude level). Such field dependence can be present in principle both in the BCS terms (through the weak dependence of the energy gap Δ_o from H_{RF} [5]) and in the residual term. In the latter case (far more often considered) the specific form of the function R_0 (H_{RF}) strongly depends on the specific mechanism considered to be relevant in determining the residual losses. Although a large number of papers in the literature have been dedicated to trying to finally solve the so-called 'Q-slope' problem [6–9], no general consensus exists and the real mechanism determining this important effect has not been fully established.

In addition to the possible field dependence of the surface resistance, another effect also has to be considered when analyzing the Q versus E_{acc} cavity data. In fact, the heat generated by the RF power dissipation can produce a temperature increase of the inner cavity superconducting layer in respect to the liquid helium bath temperature where the cavity is immersed. Using a simplified but fully effective 'one-dimensional' thermal model, as schematically reported in figure 1, the temperature difference ΔT between the inner cavity surface T and the bath temperature T_0 can be written as:

$$\Delta T = T - T_0 = \left(\frac{d}{k_m} + R_B\right) P_d. \tag{4}$$

Here d is the thickness of the cavity wall, k_m is the thermal conductivity of the superconducting cavity material and R_B represents the thermal resistance present at the interface between the cavity outer surface and the He bath.

The thermal boundary resistance R_B has an entirely different nature depending on whether it is above or below the superfluid helium transition temperature T_λ.

He_I (above T_λ) is in fact an ordinary liquid. The heat transfer from a metal surface to a pool of boiling liquid occurs via a strong and complex convective process involving the formation of bubbles. The details of the process strongly depend on many factors (surface chemistry and roughness, system geometry, etc) and the behavior is generally characterized by some degree of hysteresis [10].

In the superfluid regime, below T_λ (He_{II}), boiling is largely suppressed and the thermal boundary resistance can be identified with the Kapitza resistance R_K. Indeed, following Kapitza's original work [11], an extended theoretical and experimental activity has been carried out to fully understand and quantify the effect. The first theory of the Kapitza resistance, proposed by Khalatnikov [12], was based on the calculation of the acoustic phonon transmission mismatch at a

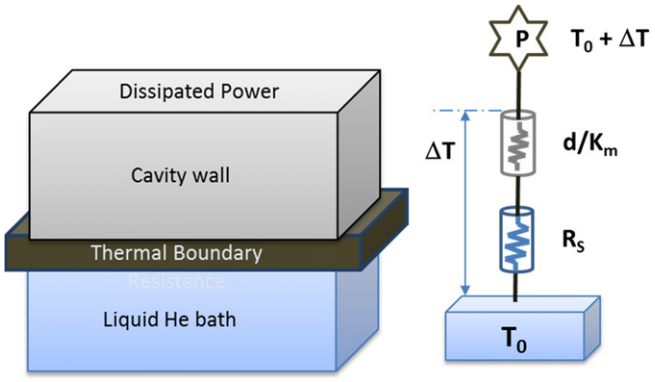

Figure 1. Electrical analog (one-dimensional model) for the heat transfer in a superconducting cavity.

perfect solid–liquid He_{II} interface. However, the predicted values for R_K were far too high compared to the experimental results. Theoretical calculations, based on the phonon diffuse scattering at a 'rough' interface (diffuse scattering model, [13]), gave results not far from the so-called 'phonon radiation limit' [14], and in this case the resulting R_K values turned out to be too low in respect to the experimental results. The latter were, in any case, not fully set, giving contradictory results between different papers and changing the measurement methodology.

It is worth mentioning that, as predicted by Landau [15], a further contribution to the boundary resistance comes from the fact that although in bulk superfluid ^{4}He the heat flux generates a counter-flow between the normal fluid and the superfluid, and no net thermal resistance is present, the counter-flow is suppressed in the vicinity of the solid wall. This 'singular' contribution becomes fairly relevant only very close (in the μK region) to T_λ [16]; its observation requires specific techniques and is not relevant to the present discussion.

In the presence of a thermal gradient between the inner cavity surface and the helium bath, the BCS surface resistance can be rewritten as:

$$R_{BCS}(T_0) = \frac{A\omega^2}{T_0 + \Delta T} \exp\left[-\frac{\Delta_0}{K_B(T_0 + \Delta T)}\right] \qquad (5)$$

with $\Delta T \propto P_d \propto H_{rf}^2$. This induces a dependence of the surface resistance on the RF field, and a corresponding Q-slope effect.

The relevance of the thermal effects described above on the accelerating cavity behavior has already been discussed in the literature. In a specific test experiment using a heater as a power source, Amrit and Francois analyzed the relative weight of the Kapitza contribution and Nb thermal conduction as a function of different Nb surface preparations at temperatures well below T_λ, concluding that the Kapitza resistance can become predominant in the thermal behavior of superconducting cavities for very clean Nb surfaces [17].

A fairly complete treatment of thermal effects has been given by Bauer *et al* [18]. In their paper the authors suggest that in order to fully describe many Q versus E_{acc} data on CEBAF 1.5 GHz cavities, at temperatures between 1.6 K and 2.0 K, the inclusion of *both* direct RF field dependence of the surface resistance and thermal effects have to be considered. In a later paper on 3.9 GHz nine-cell cavities at FERMILAB [19], using the thermal model only, a reasonable agreement with the data is instead found in the same temperature range.

However, with a few exceptions (including those mentioned above), the current assessment in the literature is that thermal effects can be essentially neglected, at least at low or moderate input power, and that the main mechanism causing the Q-slope problem is the 'direct' dependence of the surface resistance on the RF field, often invoking the RF dissipation of vortices penetrating inside the superconductor.

In the present work we present new data on the Q-factor as a function of temperature and accelerating field (input power) on small test bulk Nb 6 GHz cavities, at a wide range of temperatures and input power. The extracted R_s versus T data show in all cases a significant anomaly around T_λ; more pronounced for increasing RF power. This anomaly is often seen in the literature at the same temperature range (see, for example, the recent paper by Dhakal *et al* [20]).

In the literature the $R_s(T_o)$ data are always reported at a constant RF field. We noticed that if the $R_s(T_o)$ data are reported at constant input power, the anomaly close to the helium superfluid transition shows up as an abrupt change of the R_s value at T_λ, evidently reflecting the abrupt change of regime in the heat transmission to the He bath that indeed occurs at that temperature, due to the change from He_I to He_{II} thermal conduction regimes. This has suggested in turn that the thermal effects, though often discussed in the past, have been underestimated in the recent literature on accelerating cavities, and should be reconsidered.

In particular we will show that, from the R_s (T) experimental data, using equations (1), (4) and (5) (without assuming any explicit RF field dependence of $R_s(T)$) and through appropriate fitting procedures, it is possible to extract the absolute values and the temperature dependence of the thermal boundary (Kapitza) resistance R_B (R_K). We will show that the thermal boundary resistance obtained by this procedure exhibits values and an overall temperature dependence substantially consistent with measurements and theoretical estimations typically reported in the literature. Finally we will show that measuring cavities identical in all respects, but with different external surface treatments aimed to reduce the Kapitza thermal boundary resistance, we can get a significant improvement in terms of the Q versus E_{acc} characteristics.

The paper is organized as follows. The next section will be devoted to the description of the experimental procedures. In particular, the unique advantages of our 6 GHz cavities will be described, as well as the fabrication procedure, the different tools and techniques employed, and our cryogenic and RF measurement system.

Following that, we will present our experimental results and a discussion on the dependence of the surface resistance on temperature and RF power, in line with our results.

The discussion will make clear the possible relevance of external surface treatments in order to reduce the thermal boundary resistance and improve the overall cavity

performance. This will be shown and discussed in the last section, devoted to analyzing the effect of the external cavity surface.

The conclusion will finally summarize the obtained results and the consequent implications.

2. Experimental procedures

2.1. The 6 GHz resonators

In order to achieve higher and higher cavity performances, it is necessary to have extremely reliable manufacture protocols validated by reliable statistics from RF tests on superconducting materials. However, dealing with a large-size resonator is of high cost and time-consuming. Therefore the use of superconducting samples inside suitable test superconducting resonators is quite common. However, RF measured samples will never be comparable to a real large cavity, always being an indirect measurement.

Our strategy instead has been based on the development of small 6 GHz cavities, which are easy to handle as a sample, but remain 'real' cavities [21].

The 6 GHz cavities will produce many statistics at a lower cost and effort. Therefore, the main advantage of this method lies in it being a simple tool to open the road to new research, or to prove a phenomenon with a large number of tests at a limited cost. However, the extrapolation of quantitative information to other cavity frequencies, for instance the Q-slope versus the accelerating field, requires a deeper concern. The RF results cannot be straightforwardly scaled to lower frequencies with the square of the frequency ratio, since at 6 GHz the role of BCS losses is still very high and dominant.

Working on 6 GHz cavities has not often been considered in the past due to major technological problems using standard electron beam welding caused by the small bore of the cavity cutoff tubes.

Thanks to the spinning technology developed at INFN-LNL, our 6 GHz cavities are totally seamless [22]. Spinning is a point deformation process by which a metal disc, or a cylindrical preformed hollow component, is plastically deformed by axial or radial motions of a tool or rollers acting on a workpiece clamped against a rotating chuck. This peculiar fabrication technique is a chip-less production method of forming axially symmetrical hollow parts of almost any shape, and it is an ideal seamless fabrication technology for producing small cavities. Totally seamless cavities can be straightforwardly spun from a circular blank by this cold forming process and no intermediate annealing is required. Flanges are also directly spun together with the cavity. Kapton joints instead of the traditional indium wires are used to vacuum seal the cavity.

Our Nb 6 GHz cavities are 97 mm long and have a 45 mm diameter cell (see figure 2), an *electrical length* of 25 mm and the same geometrical factor Γ of a large resonator, equal to 287 Ω (assuming $R_S = \Gamma/Q$). The area of the central cell exposed to the RF fields is about 42 cm^2.

Figure 2. A set of 6 GHz Nb monocell cavities.

The cutoff tubes have a length equal to three times the diameter in order to damp the RF fields.

6 GHz cavities can be produced in large numbers at low cost from a relatively small amount of niobium and allow us to obtain many experimental statistics. The reason is that while a large accelerating cavity requires expensive and time-consuming treatments, due to the small size of the cavities, all the surface treatments (mechanical polishing, buffer chemical polishing, electropolishing, high-pressure rinsing, alcohol rinsing, thermal treatments and many other surface treatments such as purifications and even the RF test) can be performed quickly and at low cost. Even usage of the tool for surface treatments (tumbler, chemical plant, high-temperature furnace, cryostats) is reduced and less expensive than that for large cavities. With a tool like this, it is possible to study traditional and innovative surface treatments as well as new thin-film superconducting materials grown for example by sputtering or thermal diffusion techniques.

The spinning process implies material surface defects, stress and lattice dislocations. Obviously the internal surface finishing of a resonant structure is directly correlated to its performance, especially at high fields. In order to remove surface roughness and contaminations introduced during the spinning process, the cavity is mechanically polished by tumbling with silicon carbide media, electropolished up to the removal of 300 μm in a mixture of H_2SO_4:HF at a ratio of 9:1 with an aluminum cathode, then high-temperature annealed in UHV at 2000 °C for 60 s [23].

2.2. Cavity assembly and cryogenics

After the 100 bar deionized water rinsing, the resonators are fast mounted in a class 1000 clean room on a removable attachment as shown in figure 3. The attachment is then fixed to its own RF cryogenic vertical stand that is preliminarily pumped by a turbo-molecular pump and subsequently by an ionic pump of 2 L sec^{-1} in order to avoid vibrations once the RF cryogenic stand is plunged into the cryostat.

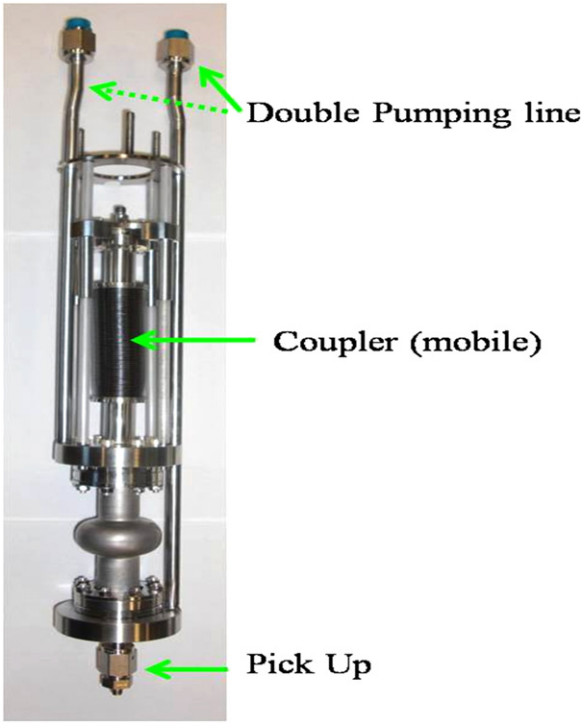

Figure 3. The cavity, equipped with a pick-up antenna and movable coupler antenna, mounted onto a removable attachment that will be mounted onto the cryogenic stand.

This removable attachment consists of two parts: a coupler top flange, equipped with an edge-welded bellow that allows the motion of the coupler antenna, and a pick-up bottom flange, equipped with an SMA coaxial feedthrough welded to the antenna that picks up the RF signal. The cavity is sealed to the a.m. flanges by 100 micron Kapton joints. The cavity is pumped through a double 8 mm diameter vacuum pumping line, passing through the coupler flange and the pick-up flange.

Since the cavity is equipped with a movable coupler, the RF measurement always uses critical coupling, thereby ensuring higher precision than when working either under-coupled or over-coupled in the fixed coupler configuration.

The stand is slowly inserted into a cryostat using an overhead traveling crane and cooled at the temperature of the liquid helium (4.2 K) for the measurement of the Q-factor versus accelerating field. After that, the bath is ready to be pumped down in pressure to gradually reach the ultimate temperature of 1.8 K in order to study the variation of cavity surface resistance as a function of the temperature.

Two Lake Shore calibrated thermometers, a silicon diode (calibrated in the range 1.4–500 K) and a negative T-coefficient germanium thermometer (calibrated in the range 0.05–100 K), immersed in the liquid helium bath at a 1 cm distance from the cavity ensure the reliability of the temperature measurement. For every temperature, the RF data acquisition is done only when the temperature is stabilized and both the thermometers measure a value within 5 hundredths of a Kelvin of each other.

2.3. The radiofrequency measurement system

The Q measurement and RF processing of the resonator take advantage of computer-controlled procedures which communicate with the devices, collect data and assist the operator during the measurements. In figure 4, a schematic diagram of the RF measurement system is shown. The computer is interfaced with the signal generator, power meters and frequency counter via an IEEE 488 bus. The auxiliary equipment (not shown) such as the helium level meter, temperature, vacuum, pressure sensors and stepping motor control are connected by an RS232 bus. The RF generator signal is divided into three paths: one goes through the programmable phase shifter to feed an LO mixer input, the second goes to the frequency counter, while the third one arrives at the power amplifier through a PIN diode switch and a programmable PIN diode attenuator. A bi-directional coupler allows monitoring of the forward and reflected powers in the feeding line that are measured by a two-channel power meter. The pick-up signal passes through a computer-controlled RF relay for sensitivity selection and a low-noise amplifier, and it is also split into two paths. The first reaches the mixer RF input through a limiting amplifier optimizing mixer performance; the second leads to a second power meter. The phase error signal, coming from the intermediate frequency mixer output, is amplified and filtered by the dc amplifier and monitored by USB control card ADC. The RF power dividers/combiners are used to organize the RF signal flow. The fixed attenuators are used to optimize the signal level in different parts of the system. We use the five-step semiautomatic calibration procedure for all the elements up to the cavity ports [24].

After that, we determine the cavity Q at a low field cavity in critical coupling. We feed the cavity, locked in phase at its resonant frequency, and adjust the coupler position to minimize the cavity reflected power. At equilibrium (stable cavity field), the Q measurement procedure is started. It turns off the power and interpolates the pick-up decay data in order to determine the cavity decay time and the related Q-value. From the Q-value and from the measure of feeding and transmitting power, the program then computes the pick-up accelerating field coefficient (known as the ratio between stored energy and the square of the accelerating field). The accelerating field and the correspondent Q-value at higher accelerating fields can then be determined by increasing the feeding power and adjusting the coupling in order to maintain the critical coupling condition. In detail, what happens is that once the temperature value is stabilized at a fixed value, the Q-factor value is acquired at different values of the RF input power. Therefore, for every temperature value, the program automatically plots the triad of Q-factor, accelerating field and RF input power values, allowing a fast recording and analysis of the data together with all the auxiliary parameters [24, 25].

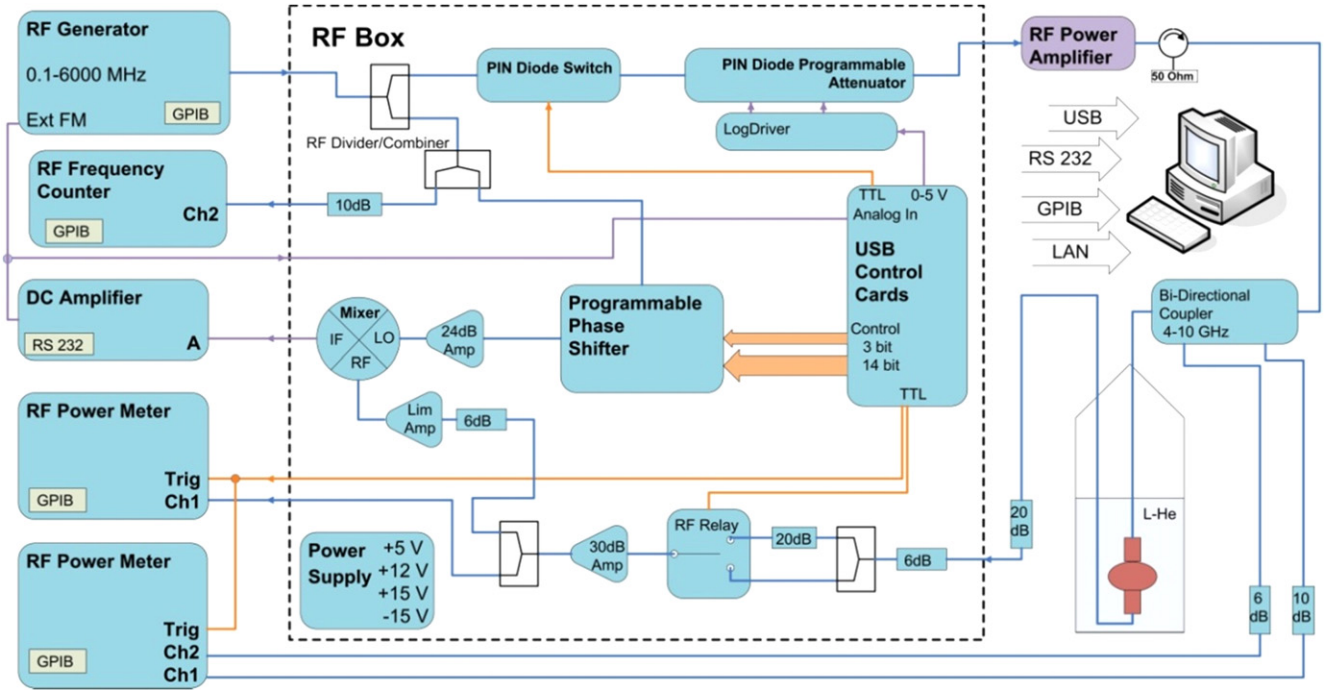

Figure 4. Schematic diagram of the RF measurement system for 6 GHz superconducting cavities.

3. Experimental results and discussion of untreated cavities

As mentioned in the introduction, the starting point of our work was to notice that in most cases the $R_s(T)$ values extracted from accelerating cavity Q-measurements reported in the literature showed a 'jump' or abrupt change just above the He_I-He_{II} transition (lambda point, $T_\lambda = 2.18\,K$, $1/T_\lambda = 0.46\,K^{-1}$) (as an example, refer to Dhakal *et al* [20]). This circumstance, also systematically found in our own measurements, is not commented on in the literature, possibly due to the simple consideration that in that temperature region some temperature instability can obviously occur. However, we noticed that if the $R_s(T)$ data are taken keeping a constant input power, the anomaly is far more clear and defined, and exhibits an abrupt change of the R_s value exactly at T_λ.

The conceptual difference between the data taken at a constant RF field or constant RF power is illustrated in figure 5. According to equation (3), if we decrease the temperature at a constant field, we will also decrease the value of the RF power; if we decrease the temperature at constant power, instead, we will increase the value of the magnetic field. Therefore the acquisition of the curve of R_S versus 1/T at a constant field will be useful for the experimental data treatment in the framework of an electrodynamic model approach. The acquisition of the same curve at constant power will be more useful in the framework of a thermal model approach.

In figure 6 the $R_s(T)$ data obtained from the Q measurements at constant RF power are reported for one of our 6 GHz Nb cavities following the experimental procedures described in the previous section.

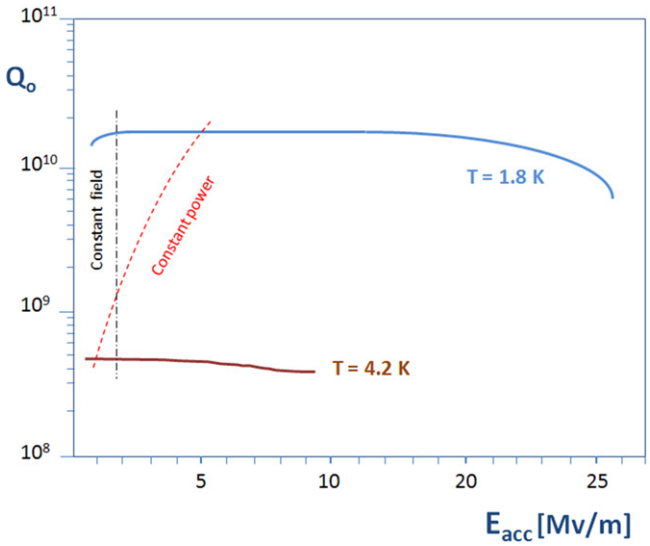

Figure 5. Conceptual difference between Q data taken at constant RF field and constant RF power.

The reported behavior is found with the same general characteristics in all our measured samples (over 140 measurements of about 100 Nb 6 GHz cavities).

We can get more insight into this behavior considering that typically reported values in the literature for the temperature difference ΔT' for heat exchange between a metallic surface and boiling liquid helium above the lambda transition are at maximum of the order of 0.1 K for input power density up to $5*10^{-3}$ W cm^{-2} [10]. This corresponds to the maximum input power level of 200 mW that we used in our measurements (this value of the power density is estimated

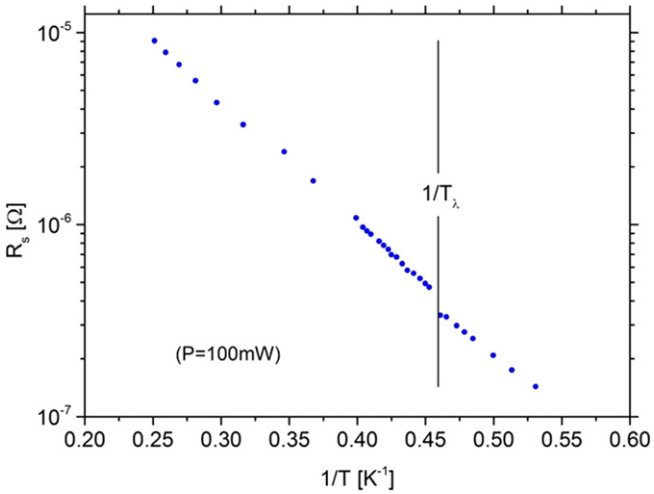

Figure 6. Surface resistance (ln scale) versus the inverse of the bath temperature. Measurements were taken at a constant RF power of 100 mW.

considering that the power input can be assumed to be uniformly distributed over a cavity surface of about 42 cm^2 for our 6 GHz cavities). Moreover, for our cavities, given the high quality of our Nb (RRR ≈ 300) and the small wall thickness ($d = 0.2$–0.3 cm), we can assume $d/k_m \leqslant 0.4\ cm^2\ K\ W^{-1}$ at 4.2 K (only moderately increasing when lowering the temperature).

Since ΔT will be much smaller below T_λ (where the thermal boundary resistance is identified with the Kapitza resistance) the condition $\Delta T \ll T$ will always be well satisfied in our measurements.

In this limit we can rewrite equation (5) as:

$$R_{BCS}(T_0) = \frac{A\omega^2}{T_0}\exp\left[-\frac{\Delta_o}{K_B T_0}\right]\left(1 + \frac{\Delta_o \cdot \Delta T}{K_B T_o^2}\right) \approx R_{BCSO}(T_0)\left(1 + \frac{\Delta_o \cdot \Delta T}{K_B T_o^2}\right) \quad (6)$$

where T_o is the bath temperature and R_{BCSO} is the BCS surface resistance in the absence of thermal effects (equation (2)). From equation (4) we know that ΔT is proportional to the input power P_d (assuming a power-independent thermal boundary resistance, which is a reasonable assumption at low or moderate input power), so we can write for the overall surface resistance:

$$R_s(T_0) = R_{BCSO}(T_o)\left(1 + \frac{\Delta_o \cdot P_d(d/k_m + R_B)}{K_B T_o^2}\right) + R_o \quad (7)$$

(here R_o is assumed to be both temperature- and RF power-independent).

Equation (7) implies that the measured surface resistance directly depends on R_B and this is clearly the only quantity in the equation possibly sensitive to the He_I–He_{II} transition: the abrupt change in R_s at T_λ observed in figure 6 can only be ascribed to a sharp change in the overall thermal boundary resistance R_B between the external cavity wall and the helium bath.

In figure 7 we report, in a 3D plot, the evolution of the observed 'jump' of $R_s(T)$ at the helium lambda transition T_λ as a function of the input power (again kept accurately constant) for a different sample. From the figure we can deduce an approximately linear dependence of the T_λ jump as a function of the input power and that the jump would disappear in the limit of zero applied RF power. Equation (7) implies indeed that the surface resistance would scale linearly with the input power P_d at a fixed bath temperature (at a rate depending on the overall thermal resistance). In particular, the temperature jump at T_λ would also be expected to depend linearly on the power, as occurs, in good approximation, with the data reported in the figure.

It is worth pointing out now that equation (7), through equation (3) $\left(P_d = \frac{1}{2}R_s(T)H_{rf}^2\right)$, implies a square dependence on the RF field of the BCS surface resistance term at any fixed temperature, as already discussed by Padamsee [26] in the frame of a similar thermal mismatch model.

Moreover, equation (3) implies that if the surface resistance measurements were performed at a constant field (and not at a constant power), the dissipated power at the cavity inner surface P_d would strongly decrease the lowering of the temperature, due to the exponential decrease of R_s. This would imply, in turn, a significant change in the observed temperature dependence of $R_s(T_o)$ as described by equation (7). In other words, the usual expression $R_s(T) = R_{BCS}(T) + R_0$, due to the finite thermal resistance, is indeed only valid in the limit of zero power input, which, of course, cannot be realized in real experiments.

Equation (7) shows that the measured surface resistance $R_s(T_o)$ directly depends on the overall thermal resistance $\frac{d}{k_m} + R_B$. Within the assumed frame it is then possible to extract this latter quantity by equation (8):

$$\frac{d}{k_m} + R_B = \frac{K_B T_0^2}{\Delta_0 P_d}\left[\frac{R_s(T_0) - R_0}{R_{BCS0}(T_0)} - 1\right] \quad (8)$$

which is simply obtained by 'inverting' equation (7).

In figure 8, curve 1 (squares), the temperature dependence of the overall thermal resistance is reported, as deduced by equation (8) using for $R_s(T_0)$ the experimental data reported in figure 6 (the two data points just below the lambda transition have been omitted in the fit due to the critical thermal instability in that region). Due to the already discussed small value of d/k_m ($\ll 1\ cm^2 K\ W^{-1}$) in our case, the overall thermal resistance is in fact coincident with the thermal boundary resistance R_B, in turn coincident with the Kapitza resistance R_K below T_λ. Given the nature of the external surface for the specific cavity under study (polished bulk Nb), the circumstance that the Kapitza resistance is the dominant term in the overall thermal resistance below T_λ is not surprising, as discussed, for example, by Amrit and Francois [17].

The parameters used in the theoretical expression for $R_{BCSO}(T_o)$ in equation (8) to obtain the overall thermal resistance are reported in table 1.

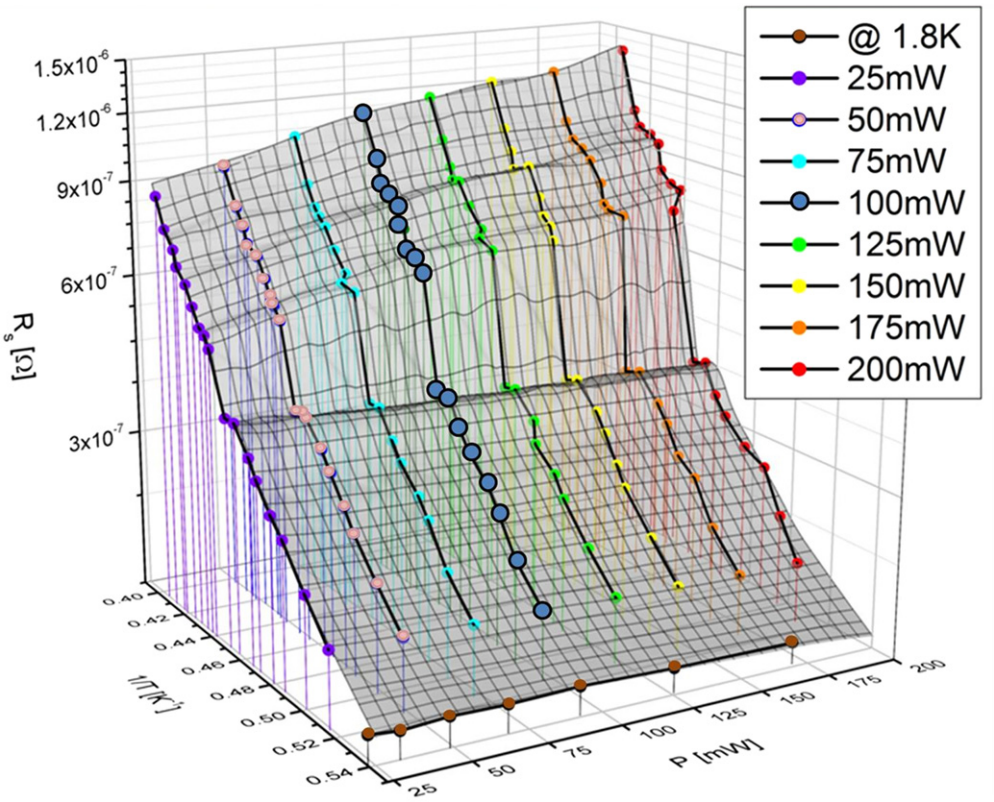

Figure 7. 3D plot of the surface resistance as a function of inverse bath temperature and RF power.

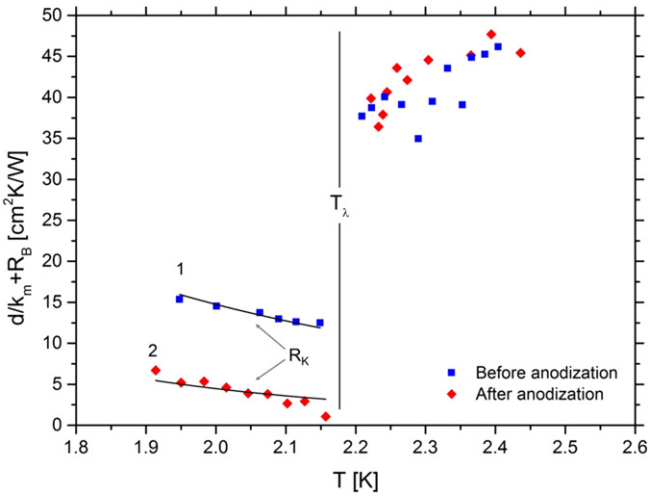

Figure 8. Temperature dependence of the overall thermal boundary resistance, as deduced by our surface resistance measurements, on a typical Nb 6 GHz cavity. Curve 1 (squares): polished Nb surface (current section). Curve 2 (diamonds): externally anodized Nb surface (next section).

Table 1. List of parameters used in the theoretical expression of $R_{BCSO}(T_o)$.

Δ_o	$A\omega^2$	R_o
1.40 meV	2.18 10^{-3} Ω*K	20 nΩ

Δ_o and the parameter $A\omega^2$ were determined by extrapolating to zero power the classical BCS fitting of the R_s curves in the high-temperature region obtained at constant decreasing power. This is justified by equation (7), showing that for $R_s \gg R_o$ and $P_d \rightarrow 0$ we get $R_{BCSO}(T_o) = R_s(T_o)$. The reported value of Δ_o implies $\Delta_o/K_B T_c = 1.76$, very close to the theoretical BCS value.

The value of the residual resistance R_o cannot be easily deduced by the same procedure and has been chosen to ensure that the low-temperature data (below T_λ) for the thermal boundary resistance follow a T^{-3} dependence, as theoretically predicted for the Kapitza resistance (continuous fitting curve in the figure).

The T^{-3} dependence of the Kapitza resistance [12–14] is indeed set on fairly solid grounds, simply reflecting the change in temperature of the overall phonon number in the solid at low temperatures. The parameters reflecting the solid/He_{II} interface nature determining the specific phonon interface scattering mechanisms between the two well-known limits of (1) a perfectly reflecting surface (acoustic mismatch model) and (2) a rough surface (diffuse mismatch model, which gives results close to the so-called 'perfect matching limit') should be essentially temperature-independent.

It is worth underlining that, although the described procedure has some degree of arbitrariness, the deduced temperature dependence of the thermal resistance is relatively sensitive to the precise choice of the power law exponent: as an example, the assumption of a $T^{-4.5}$ temperature dependence of the Kapitza resistance, as assumed on the basis of

experimental evidence, for example, by Bauer *et al* [18], would hardly change the value of R_o or the overall shape and absolute values of the deduced thermal resistance curve.

It is also important to notice that the absolute values of the thermal resistance both above and below the lambda point are not far from the data reported in the literature for heat transfer to pool boiling He_I above T_λ [10] and for the Kapitza interface resistance (below T_λ) between a polished metal surface and superfluid He_{II} [13, 14, 17], and lie well within the theoretical limits of about 35 $cm^2K\,W^{-1}$ for Nb at T = 2 K in the acoustic mismatch model and 1 $cm^2K\,W^{-1}$ in the phonon radiation limit.

Finally, as already discussed in the introduction, the temperature measurement sensitivity in our case is certainly not sufficient to observe the effects predicted by Landau [15], that indeed occur in a very narrow temperature range around T_λ [16].

4. Effect of external cavity surface treatments

In the previous section we discussed and attempted to demonstrate the relevant role of thermal effects on the surface resistance $R_s(T,P_d)$ and in turn on the quality factor Q. We also demonstrated that, assuming a temperature- and field-independent low-temperature residual resistivity and the thermal boundary resistance reported in figure 8, curve 1, we can perfectly describe our R_s data as a function of temperature and power. The obvious consequence of this is, of course, to attempt to reduce the thermal boundary resistance, in order to improve the overall cavity performance.

In fact, data in the literature clearly indicate that the Kapitza boundary resistance strongly depends on surface treatments, being lower for etched or generally rougher surfaces [17]. In the frame of the theory of the Kapitza resistance, this can be ascribed to the fact that a rougher surface should tend to 'diffuse scattering model' behavior (in contrast to a specular surface, which should tend to 'acoustic mismatch model' behavior), characterized by a lower Kapitza thermal resistance. In addition, the introduction of a different material layer between Nb and the He_{II} bath should reduce the Kapitza resistance, if the intermediate material presents an 'acoustic impedance' $Z = \rho v_o$ (ρ is the material density and v_o is the sound velocity) between Nb and He_{II}, allowing a degree of 'impedance matching' for the phonon propagation at the interface [14]. Moreover, we cannot exclude that effects related to boiling processes are still active below T_λ. Those processes would certainly be strongly influenced by the surface roughness [27].

In figure 9 we report the surface resistance versus the inverse of the bath temperature at constant RF power for the same cavity reported in figure 6, after an electrolytic pad anodization process that grew, externally to the cavity surface, a blue porous Nb oxide a few tenths of a nanometer thick. The process did not influence the inner cavity surface in any case. In fact, the 6 GHz Nb cavity was initially measured at low temperatures, then extracted from liquid helium, warmed up to room temperature and then subject to external anodized cycling, keeping it under UHV. The anodization of the cavity external wall was done at room temperature by a movable electrode covered by a sponge wet in a water-diluted solution of 30 g l^{-1} citric acid at a potential of 26 Volts. The color depends on the applied voltage. The anodization of the cavity exterior was performed until the niobium became an intense blue color. It is important to always keep the cavity under UHV during the coloring. The cavity was then cooled down to low temperature again and RF tested.

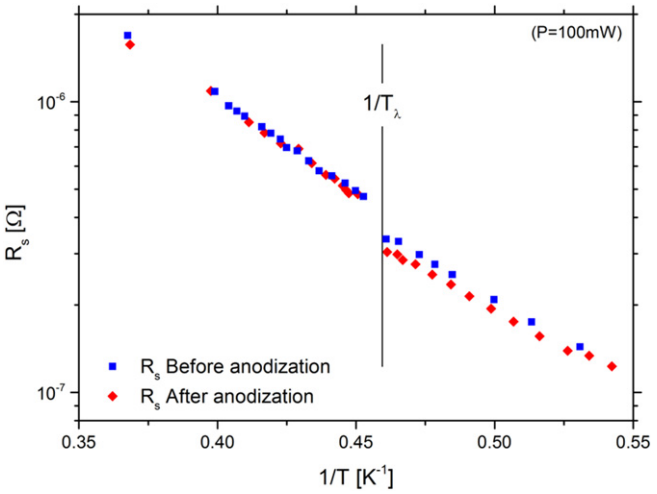

Figure 9. Surface resistance at constant RF power versus the inverse of the bath temperature around the He_{II} lambda transition before (squares) and after (diamonds) the external anodization process (see text). The data before anodization are the same as already discussed in figure 6.

The data reported in figure 9 show a significant lowering of the surface resistance below the helium lambda transition, corresponding to an increase of the quality factor Q. This is evidently due to a lowering of the Kapitza resistance. The external treatment did not influence the R_s values above T_λ as expected due to the nature of the thermal boundary resistance in that temperature region (due, as already mentioned, to a strong convective process involving the formation of bubbles).

The data points reported in figure 8, curve 2, refer to the same 6 GHz cavity whose behavior was reported in the previous section, and have been obtained by equation (8) using the surface resistance data reported in figure 9, i.e. after the external surface anodization process. The parameters used to obtain the data from equation (8) are the same used to extract curve 1, and reported in table 1. Indeed, the external anodization treatment, as discussed above, has no possible influence on the superconducting properties of the inner surface.

The observed reduction of the Kapitza resistance below T_λ due to the different states of the external surface (from a polished surface to a 'rough' one) is consistent with many reports from the literature [17, 27]. However, it is worthwhile to note that all of our experimental measurements show a parallel shift of the Q versus E_{acc} curve and do not seem to affect the Q-slope in the way described by many authors [27–30].

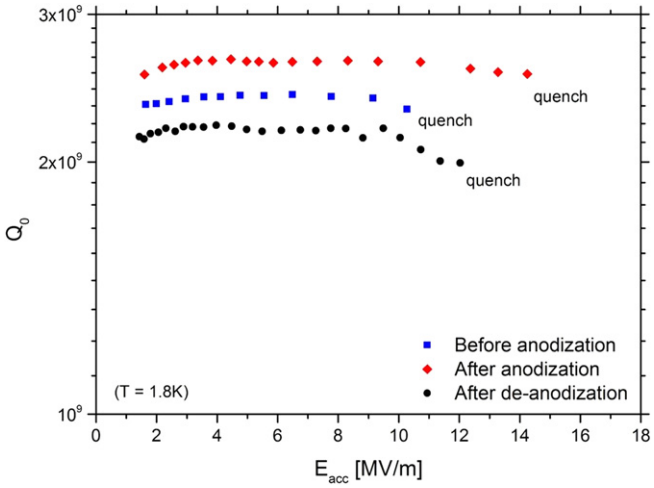

Figure 10. RF test of the cavity of figure 9. The squares refer to the cavity prepared in a standard way. The diamonds refer to the same cavity after anodization of the external surface. The circles refer to the same cavity after the stripping of the external anodization.

As reported in figure 10 (which refers to the same cavity as figure 9), the external blue anodization process increases both the Q-factor and the accelerating field.

When the anodized layer is further removed we see that Q is again lowered to a level even lower than it was before anodization. We suppose that the reason for this is that the blue oxide layer is removed chemically in a mixture of HF, H_2NO_3 and H_3PO_4 at a 1:1:4 ratio. After the chemistry, the cavity external surface is shining, and we have observed in further experiments that the specularity of the external surface negatively affects the cavity performance. As already discussed, a mirror-like surface acts as a mirror for phonons, producing a higher acoustic mismatch and, in turn, a higher Kapitza resistance.

Analogous results were found in several tests on different cavities. It is important to note that all operations were done without breaking the vacuum and that the movable coupler allowed us to perform high-precision measurements.

5. Conclusions

From this paper we can extract some important conclusions, rather new in the panorama of RF superconductivity.

We have discovered the presence of a steep jump in the surface resistance versus temperature curve at the superfluid transition temperature T_λ of liquid helium, when measuring at fixed input power rather than at a fixed accelerating field (in the latter case the jump is seen as a much smoother anomaly). This jump clearly indicates that the losses abruptly decrease at the superfluid transition, and that the external environment is fundamental for the thermal exchange. This conclusion can appear obvious, but in practice in the literature, attention has always been focused on the effect of the RF fields on the internal surface of the Nb cavity, considering the approximation in which the latter is in contact with an infinite reservoir of liquid helium with infinite thermal conductivity.

We have seen that when injecting more RF power in the cavity, the jump increases, indicating that the thermal exchange with the He bath becomes more and more important, and, in turn, that thermal boundary resistance effects become more and more important.

From the experimental data acquired, we have found a new way to extract the thermal boundary resistance (i.e. the Kapitza resistance below T_λ). We have shown that a superconducting cavity can be a valid alternative for measuring Kapitza resistance, since it is a quasi-spherical system confining the RF heat load almost uniformly inside itself, and above all without the edge effects that affect thermal devices generally used to measure Kapitza resistance. The extracted values are compatible (on the higher side) with current literature data for the thermal boundary resistance both above and below T_λ. We then tested different external surface treatments on the cavity aimed at reducing the Kapitza resistance, and proved that electrolytic pad anodization, producing porous Nb oxide a few tenths of a nanometer thick on the external cavity wall (without affecting the internal cavity surface in any way), systematically and significantly lowers the Kapitza resistance and, in turn, the measured surface resistance below T_λ, improving the overall Q versus E_{acc} cavity performance at the operating temperature.

Acknowledgements

The authors are indebted to F Stivanello for the chemical and electrochemical treatments, M Checchin and M Martinello for their help in RF tests, R K Thakur, G Yu and A Battistello for the mechanical finishing of the 6 GHz cavities, and C Pira for assistance in editing the paper. The research was developed in the framework of the NTA-SHAMASH Experiment funded by the 5th National Board of INFN.

References

[1] Schmüser P 2003 Basic principles of RF superconductivity and superconducting cavities *Proc. of CERN Accelerator School in Zeuthen*
[2] Halbritter Z 1974 *Phys.* **266** 209
[3] Klopman B 1993 *PhD Thesis* University of Twente
[4] Andreone A *et al* 1993 *J. Appl. Phys.* **73** 4500
[5] Palmieri V 2005 The problem of Q-drop in superconducting resonators revised by the analysis of fundamental concepts from RF superconductivity theory *Proc. of the XII Int. Workshop on RF Superconductivity* (Ithaca: Cornell University) (http://lns.cornell.edu/public/SRF2005/pdfs/TuA02.pdf)
[6] Visentin B *et al* 1998 Improvements of superconducting cavity performances at high accelerating gradients *Proc. of the 6th EPAC* vol 3 (Stockholm, Sweden) p1885
Visentin B 2006 Low, medium, high field Q-Slopes change with surface treatments *ICFA Beam Dynamics Newsletter no. 39* 94–106
[7] Ciovati G 2006 High Q at low and medium field *ICFA Beam Dynamics Newsletter no. 39* 80–93 (http://icfa-usa.jlab.org/archive/newsletter/icfa_bd_nl_39.pdf)

[8] Eremeev G and Padamsee H 2006 Change in high field Q-slope by baking and anodizing *Physica* C **441** 62–5
[9] Attanasio C, Maritato L and Vaglio R 1991 *Phys. Rev.* B **43** 6121
[10] Van Sciver S 2011 *Helium Cryogenics* (New York: Springer)
[11] Kapitza P L 1941 *J. Phys. USSR* **4** 181
[12] Khalatnikov I M 1965 *Introduction to the Theory of Superfluidity* (New York: Benjamin)
[13] Swartz E P and Pohl R O 1989 *Rev. Mod. Phys.* **61** 605
[14] Snyder N S 1970 *Cryogenics* **10** 89–95
[15] Landau L D 1941 *J. Phys. USSR* **71**
[16] Duncan R V *et al* 1987 *Phys. Rev. Lett.* **58** 377
[17] Amrit J and Francois M X 2000 *J. Low Temp. Phys.* **119** 27
[18] Bauer P *et al* 2006 *Physica* C **C441** 51
[19] Edwards H, Cooper C A, Ge M, Gonin I V, Harms E R and Khabiboulline T N S 2009 Comparison of buffered chemical polished and electropolished 3.9 GHz cavities TUPPO063 *Proc. of SRF2009* ed J Knobloch (Berlin, Germany) (http://accelconf.web.cern.ch/AccelConf/SRF2009/papers/tuppo063.pdf)
[20] Dhakal *et al* 2013 *Phys Rev Sp. Top* **16** 041001
[21] Badan L, Durand C, Palmieri V, Preciso R, Stark S, Stivanello F and Venturini W 1998 RF characterization of small scale cavities *Particle Accelerators* **62** 637–43
[22] Palmieri V, Preciso R, Ruzinov V L, Stark S Y and Gambalonga S 1994 Forming of seamless accelerating resonators of the reentrant type by the spinning technique *Nucl. Instrum. Methods Phys. Res.* A **342** 353–6
[23] Rossi A A, Thakur R K, Checchin M, Stivanello F, Yu G, Battistello A, Stark S and Palmieri V V 2013 Purification of 6 GHz cavities by induction heating *Proc. of SRF TUIOC05* ed G Martinet and C Antoine (Paris)
[24] Stark S, Porcellato A M, Rossi A A and Palmieri V 2013 Recent upgrade of ultra-broadband RF system for cavity characterization *Proc. of SRF THP096* ed G Martinet and C Antoine (Paris)
[25] Stark S, Bisoffi G, Boscagli L, Palmieri V and Porcellato A M 2004 New RF measuring system for cavity characterization *Proc. of EPAC (Lucerne, Switzerland)* pp 692–4
[26] Padamsee H, Knobloch J and Hays T 1998 *Rf Superconductivity for Accelerators* (Wiley Series in Beam Physics and Accelerator Technology) (New York: Wiley-VCH)
[27] Mikhail N R 1952 *PhD. Thesis* Imperial College of Science and Technology (London)
[28] Romanenko A, Grassellino A, Barkov F and Ozelis J P 2013 Effect of mild baking on superconducting niobium cavities investigated by sequential nanoremoval *Phys. Rev. ST Accel. Beams* **16** 012001
[29] Xiao B P, Reece C E and Kelley M J 2013 Superconducting surface impedance under radiofrequency field *Physica C: Superconductivity* **490** 26–31
[30] Grassellino A, Romanenko A, Melnychuk O, Trenikhina Y, Crawford A, Rowe A, Wong M, Sergatskov D, Khabiboulline T and Barkov F 2013 Nitrogen and argon doping of niobium for superconducting radio frequency cavities: a pathway to highly efficient accelerating structures *Supercond. Sci. Technol.* **26** 102001